# Search for $D^0 \to \gamma\gamma$ and improved measurement of the branching fraction for $D^0 \to \pi^0\pi^0$

M. Ablikim,[1] M. N. Achasov,[9,a] X. C. Ai,[1] O. Albayrak,[5] M. Albrecht,[4] D. J. Ambrose,[44] A. Amoroso,[48a,48c] F. F. An,[1] Q. An,[45] J. Z. Bai,[1] R. Baldini Ferroli,[20a] Y. Ban,[31] D. W. Bennett,[19] J. V. Bennett,[5] M. Bertani,[20a] D. Bettoni,[21a] J. M. Bian,[43] F. Bianchi,[48a,48c] E. Boger,[23,h] O. Bondarenko,[25] I. Boyko,[23] R. A. Briere,[5] H. Cai,[50] X. Cai,[1] O. Cakir,[40a,b] A. Calcaterra,[20a] G. F. Cao,[1] S. A. Cetin,[40b] J. F. Chang,[1] G. Chelkov,[23,c] G. Chen,[1] H. S. Chen,[1] H. Y. Chen,[2] J. C. Chen,[1] M. L. Chen,[1] S. J. Chen,[29] X. Chen,[1] X. R. Chen,[26] Y. B. Chen,[1] H. P. Cheng,[17] X. K. Chu,[31] G. Cibinetto,[21a] D. Cronin-Hennessy,[43] H. L. Dai,[1] J. P. Dai,[34] A. Dbeyssi,[14] D. Dedovich,[23] Z. Y. Deng,[1] A. Denig,[22] I. Denysenko,[23] M. Destefanis,[48a,48c] F. De Mori,[48a,48c] Y. Ding,[27] C. Dong,[30] J. Dong,[1] L. Y. Dong,[1] M. Y. Dong,[1] S. X. Du,[52] P. F. Duan,[1] J. Z. Fan,[39] J. Fang,[1] S. S. Fang,[1] X. Fang,[45] Y. Fang,[1] L. Fava,[48b,48c] F. Feldbauer,[22] G. Felici,[20a] C. Q. Feng,[45] E. Fioravanti,[21a] M. Fritsch,[14,22] C. D. Fu,[1] Q. Gao,[1] X. Y. Gao,[2] Y. Gao,[39] Z. Gao,[45] I. Garzia,[21a] C. Geng,[45] K. Goetzen,[10] W. X. Gong,[1] W. Gradl,[22] M. Greco,[48a,48c] M. H. Gu,[1] Y. T. Gu,[12] Y. H. Guan,[1] A. Q. Guo,[1] L. B. Guo,[28] Y. Guo,[1] Y. P. Guo,[22] Z. Haddadi,[25] A. Hafner,[22] S. Han,[50] Y. L. Han,[1] X. Q. Hao,[15] F. A. Harris,[42] K. L. He,[1] Z. Y. He,[30] T. Held,[4] Y. K. Heng,[1] Z. L. Hou,[1] C. Hu,[28] H. M. Hu,[1] J. F. Hu,[48a,48c] T. Hu,[1] Y. Hu,[1] G. M. Huang,[6] G. S. Huang,[45] H. P. Huang,[50] J. S. Huang,[15] X. T. Huang,[33] Y. Huang,[29] T. Hussain,[47] Q. Ji,[1] Q. P. Ji,[30] X. B. Ji,[1] X. L. Ji,[1] L. L. Jiang,[1] L. W. Jiang,[50] X. S. Jiang,[1] J. B. Jiao,[33] Z. Jiao,[17] D. P. Jin,[1] S. Jin,[1] T. Johansson,[49] A. Julin,[43] N. Kalantar-Nayestanaki,[25] X. L. Kang,[1] X. S. Kang,[30] M. Kavatsyuk,[25] B. C. Ke,[5] R. Kliemt,[14] B. Kloss,[22] O. B. Kolcu,[40b,d] B. Kopf,[4] M. Kornicer,[42] W. Kühn,[24] A. Kupsc,[49] W. Lai,[1] J. S. Lange,[24] M. Lara,[19] P. Larin,[14] C. Leng,[48c] C. H. Li,[1] Cheng Li,[45] D. M. Li,[52] F. Li,[1] G. Li,[1] H. B. Li,[1] J. C. Li,[1] Jin Li,[32] K. Li,[13] K. Li,[33] Lei Li,[3] P. R. Li,[41] T. Li,[33] W. D. Li,[1] W. G. Li,[1] X. L. Li,[33] X. M. Li,[12] X. N. Li,[1] X. Q. Li,[30] Z. B. Li,[38] H. Liang,[45] Y. F. Liang,[36] Y. T. Liang,[24] G. R. Liao,[11] D. X. Lin,[14] B. J. Liu,[1] C. X. Liu,[1] F. H. Liu,[35] Fang Liu,[1] Feng Liu,[6] H. B. Liu,[12] H. H. Liu,[1] H. H. Liu,[16] H. M. Liu,[1] J. Liu,[1] J. P. Liu,[50] J. Y. Liu,[1] K. Liu,[39] K. Y. Liu,[27] L. D. Liu,[31] P. L. Liu,[1] Q. Liu,[41] S. B. Liu,[45] X. Liu,[26] X. X. Liu,[41] Y. B. Liu,[30] Z. A. Liu,[1] Zhiqiang Liu,[1] Zhiqing Liu,[22] H. Loehner,[25] X. C. Lou,[1,e] H. J. Lu,[17] J. G. Lu,[1] R. Q. Lu,[18] Y. Lu,[1] Y. P. Lu,[1] C. L. Luo,[28] M. X. Luo,[51] T. Luo,[42] X. L. Luo,[1] M. Lv,[1] X. R. Lyu,[41] F. C. Ma,[27] H. L. Ma,[1] L. L. Ma,[33] Q. M. Ma,[1] S. Ma,[1] T. Ma,[1] X. N. Ma,[30] X. Y. Ma,[1] F. E. Maas,[14] M. Maggiora,[48a,48c] Q. A. Malik,[47] Y. J. Mao,[31] Z. P. Mao,[1] S. Marcello,[48a,48c] J. G. Messchendorp,[25] J. Min,[1] T. J. Min,[1] R. E. Mitchell,[19] X. H. Mo,[1] Y. J. Mo,[6] C. Morales Morales,[14] K. Moriya,[19] N. Yu. Muchnoi,[9,a] H. Muramatsu,[43] Y. Nefedov,[23] F. Nerling,[14] I. B. Nikolaev,[9,a] Z. Ning,[1] S. Nisar,[8] S. L. Niu,[1] X. Y. Niu,[1] S. L. Olsen,[32] Q. Ouyang,[1] S. Pacetti,[20b] P. Patteri,[20a] M. Pelizaeus,[4] H. P. Peng,[45] K. Peters,[10] J. Pettersson,[49] J. L. Ping,[28] R. G. Ping,[1] R. Poling,[43] Y. N. Pu,[18] M. Qi,[29] S. Qian,[1] C. F. Qiao,[41] L. Q. Qin,[33] N. Qin,[50] X. S. Qin,[1] Y. Qin,[31] Z. H. Qin,[1] J. F. Qiu,[1] K. H. Rashid,[47] C. F. Redmer,[22] H. L. Ren,[18] M. Ripka,[22] G. Rong,[1] X. D. Ruan,[12] V. Santoro,[21a] A. Sarantsev,[23,f] M. Savrié,[21b] K. Schoenning,[49] S. Schumann,[22] W. Shan,[31] M. Shao,[45] C. P. Shen,[2] P. X. Shen,[30] X. Y. Shen,[1] H. Y. Sheng,[1] W. M. Song,[1] X. Y. Song,[1] S. Sosio,[48a,48c] S. Spataro,[48a,48c] G. X. Sun,[1] J. F. Sun,[15] S. S. Sun,[1] Y. J. Sun,[45] Y. Z. Sun,[1] Z. J. Sun,[1] Z. T. Sun,[19] C. J. Tang,[36] X. Tang,[1] I. Tapan,[40c] E. H. Thorndike,[44] M. Tiemens,[25] D. Toth,[43] M. Ullrich,[24] I. Uman,[40b] G. S. Varner,[42] B. Wang,[30] B. L. Wang,[41] D. Wang,[31] D. Y. Wang,[31] K. Wang,[1] L. L. Wang,[1] L. S. Wang,[1] M. Wang,[33] P. Wang,[1] P. L. Wang,[1] Q. J. Wang,[1] S. G. Wang,[31] W. Wang,[1] X. F. Wang,[39] Y. D. Wang,[14] Y. F. Wang,[1] Y. Q. Wang,[22] Z. Wang,[1] Z. G. Wang,[1] Z. H. Wang,[45] Z. Y. Wang,[1] T. Weber,[22] D. H. Wei,[11] J. B. Wei,[31] P. Weidenkaff,[22] S. P. Wen,[1] U. Wiedner,[4] M. Wolke,[49] L. H. Wu,[1] Z. Wu,[1] L. G. Xia,[39] Y. Xia,[18] D. Xiao,[1] Z. J. Xiao,[28] Y. G. Xie,[1] Q. L. Xiu,[1] G. F. Xu,[1] L. Xu,[1] Q. J. Xu,[13] Q. N. Xu,[41] X. P. Xu,[37] L. Yan,[45] W. B. Yan,[45] W. C. Yan,[45] Y. H. Yan,[18] H. X. Yang,[1] L. Yang,[50] Y. Yang,[6] Y. X. Yang,[11] H. Ye,[1] M. Ye,[1] M. H. Ye,[7] J. H. Yin,[1] B. X. Yu,[1] C. X. Yu,[30] H. W. Yu,[31] J. S. Yu,[26] C. Z. Yuan,[1] W. L. Yuan,[29] Y. Yuan,[1] A. Yuncu,[40b,g] A. A. Zafar,[47] A. Zallo,[20a] Y. Zeng,[18] B. X. Zhang,[1] B. Y. Zhang,[1] C. Zhang,[29] C. C. Zhang,[1] D. H. Zhang,[1] H. H. Zhang,[38] H. Y. Zhang,[1] J. J. Zhang,[1] J. L. Zhang,[1] J. Q. Zhang,[1] J. W. Zhang,[1] J. Y. Zhang,[1] J. Z. Zhang,[1] K. Zhang,[1] L. Zhang,[1] S. H. Zhang,[1] X. Y. Zhang,[33] Y. Zhang,[1] Y. H. Zhang,[1] Y. T. Zhang,[45] Z. H. Zhang,[6] Z. P. Zhang,[45] Z. Y. Zhang,[50] G. Zhao,[1] J. W. Zhao,[1] J. Y. Zhao,[1] J. Z. Zhao,[1] Lei Zhao,[45] Ling Zhao,[1] M. G. Zhao,[30] Q. Zhao,[1] Q. W. Zhao,[1] S. J. Zhao,[52] T. C. Zhao,[1] X. H. Zhao,[29] Y. B. Zhao,[1] Z. G. Zhao,[45] A. Zhemchugov,[23,h] B. Zheng,[46] J. P. Zheng,[1] W. J. Zheng,[33] Y. H. Zheng,[41] B. Zhong,[28] L. Zhou,[1] Li Zhou,[30] X. Zhou,[50] X. K. Zhou,[45] X. R. Zhou,[45] X. Y. Zhou,[1] K. Zhu,[1] K. J. Zhu,[1] S. Zhu,[1] X. L. Zhu,[39] Y. C. Zhu,[45] Y. S. Zhu,[1] Z. A. Zhu,[1] J. Zhuang,[1] L. Zotti,[48a,48c] B. S. Zou,[1] and J. H. Zou[1]

(BESIII Collaboration)

[1]*Institute of High Energy Physics, Beijing 100049, People's Republic of China*
[2]*Beihang University, Beijing 100191, People's Republic of China*
[3]*Beijing Institute of Petrochemical Technology, Beijing 102617, People's Republic of China*
[4]*Bochum Ruhr-University, D-44780 Bochum, Germany*
[5]*Carnegie Mellon University, Pittsburgh, Pennsylvania 15213, USA*

 

[6]*Central China Normal University, Wuhan 430079, People's Republic of China*
[7]*China Center of Advanced Science and Technology, Beijing 100190, People's Republic of China*
[8]*COMSATS Institute of Information Technology, Lahore, Defence Road, Off Raiwind Road, 54000 Lahore, Pakistan*
[9]*G.I. Budker Institute of Nuclear Physics SB RAS (BINP), Novosibirsk 630090, Russia*
[10]*GSI Helmholtzcentre for Heavy Ion Research GmbH, D-64291 Darmstadt, Germany*
[11]*Guangxi Normal University, Guilin 541004, People's Republic of China*
[12]*GuangXi University, Nanning 530004, People's Republic of China*
[13]*Hangzhou Normal University, Hangzhou 310036, People's Republic of China*
[14]*Helmholtz Institute Mainz, Johann-Joachim-Becher-Weg 45, D-55099 Mainz, Germany*
[15]*Henan Normal University, Xinxiang 453007, People's Republic of China*
[16]*Henan University of Science and Technology, Luoyang 471003, People's Republic of China*
[17]*Huangshan College, Huangshan 245000, People's Republic of China*
[18]*Hunan University, Changsha 410082, People's Republic of China*
[19]*Indiana University, Bloomington, Indiana 47405, USA*
[20a]*INFN Laboratori Nazionali di Frascati, I-00044, Frascati, Italy*
[20b]*INFN and University of Perugia, I-06100 Perugia, Italy*
[21a]*INFN Sezione di Ferrara, I-44122, Ferrara, Italy*
[21b]*University of Ferrara, I-44122, Ferrara, Italy*
[22]*Johannes Gutenberg University of Mainz, Johann-Joachim-Becher-Weg 45, D-55099 Mainz, Germany*
[23]*Joint Institute for Nuclear Research, 141980 Dubna, Moscow region, Russia*
[24]*Justus Liebig University Giessen, II. Physikalisches Institut, Heinrich-Buff-Ring 16, D-35392 Giessen, Germany*
[25]*KVI-CART, University of Groningen, NL-9747 AA Groningen, Netherlands*
[26]*Lanzhou University, Lanzhou 730000, People's Republic of China*
[27]*Liaoning University, Shenyang 110036, People's Republic of China*
[28]*Nanjing Normal University, Nanjing 210023, People's Republic of China*
[29]*Nanjing University, Nanjing 210093, People's Republic of China*
[30]*Nankai University, Tianjin 300071, People's Republic of China*
[31]*Peking University, Beijing 100871, People's Republic of China*
[32]*Seoul National University, Seoul, 151-747 Korea*
[33]*Shandong University, Jinan 250100, People's Republic of China*
[34]*Shanghai Jiao Tong University, Shanghai 200240, People's Republic of China*
[35]*Shanxi University, Taiyuan 030006, People's Republic of China*
[36]*Sichuan University, Chengdu 610064, People's Republic of China*
[37]*Soochow University, Suzhou 215006, People's Republic of China*
[38]*Sun Yat-Sen University, Guangzhou 510275, People's Republic of China*
[39]*Tsinghua University, Beijing 100084, People's Republic of China*
[40a]*Istanbul Aydin University, 34295 Sefakoy, Istanbul, Turkey*
[40b]*Dogus University, 34722 Istanbul, Turkey*
[40c]*Uludag University, 16059 Bursa, Turkey*
[41]*University of Chinese Academy of Sciences, Beijing 100049, People's Republic of China*
[42]*University of Hawaii, Honolulu, Hawaii 96822, USA*
[43]*University of Minnesota, Minneapolis, Minnesota 55455, USA*
[44]*University of Rochester, Rochester, New York 14627, USA*
[45]*University of Science and Technology of China, Hefei 230026, People's Republic of China*
[46]*University of South China, Hengyang 421001, People's Republic of China*
[47]*University of the Punjab, Lahore 54590, Pakistan*
[48a]*University of Turin, I-10125, Turin, Italy*
[48b]*University of Eastern Piedmont, I-15121 Alessandria, Italy*

[a]Also at the Novosibirsk State University, Novosibirsk, 630090, Russia.
[b]Also at Ankara University, 06100 Tandogan, Ankara, Turkey.
[c]Also at the Moscow Institute of Physics and Technology, Moscow 141700, Russia and at the Functional Electronics Laboratory, Tomsk State University, Tomsk, 634050, Russia.
[d]Currently at Istanbul Arel University, 34295 Istanbul, Turkey.
[e]Also at University of Texas at Dallas, Richardson, Texas 75083, USA.
[f]Also at the NRC "Kurchatov Institute", PNPI, 188300, Gatchina, Russia
[g]Also at Bogazici University, 34342 Istanbul, Turkey.
[h]Also at the Moscow Institute of Physics and Technology, Moscow 141700, Russia.

[48c]INFN, I-10125 Turin, Italy
[49]Uppsala University, Box 516, SE-75120 Uppsala, Sweden
[50]Wuhan University, Wuhan 430072, People's Republic of China
[51]Zhejiang University, Hangzhou 310027, People's Republic of China
[52]Zhengzhou University, Zhengzhou 450001, People's Republic of China
(Received 12 May 2015; published 26 June 2015)

Using 2.92 fb$^{-1}$ of electron-positron annihilation data collected at $\sqrt{s} = 3.773$ GeV with the BESIII detector, we report the results of a search for the flavor-changing neutral current process $D^0 \to \gamma\gamma$ using a double-tag technique. We find no signal and set an upper limit at 90% confidence level for the branching fraction of $\mathcal{B}(D^0 \to \gamma\gamma) < 3.8 \times 10^{-6}$. We also investigate $D^0$-meson decay into two neutral pions, obtaining a branching fraction of $\mathcal{B}(D^0 \to \pi^0\pi^0) = (8.24 \pm 0.21(\text{stat}) \pm 0.30(\text{syst})) \times 10^{-4}$, the most precise measurement to date and consistent with the current world average.

DOI: 10.1103/PhysRevD.91.112015 PACS numbers: 12.60.-i, 13.20.-v, 13.20.Fc, 13.25.Ft

## I. INTRODUCTION

In the standard model (SM), the flavor-changing neutral current (FCNC) decay $D^0 \to \gamma\gamma$ is strongly suppressed by the Glashow-Iliopoulos-Maiani mechanism [1]. The branching fraction for $D^0 \to \gamma\gamma$ from short-distance contributions, such as an electromagnetic penguin transition, is predicted to be $3 \times 10^{-11}$ [2–4]. Long-distance contributions due to a vector meson coupling to a photon are expected to enhance the branching fraction to the range $(1\text{–}3) \times 10^{-8}$ [3,4]. These predictions are orders of magnitude beyond the reach of current experiments, but some extensions to the SM can enhance FCNC processes by many orders of magnitude. For example, in the framework of the minimal supersymmetric SM, gluino exchange can increase the branching fraction for the $c \to u\gamma$ transition to $6 \times 10^{-6}$ [5,6].

The previous experimental studies of $D^0 \to \gamma\gamma$ were performed by the CLEO and *BABAR* experiments using data samples collected at the $\Upsilon(4S)$ peak [7,8]. With an integrated luminosity of 470.5 fb$^{-1}$, corresponding to more than 250 million $D^0$ mesons based on the quoted number of reconstructed $D^0 \to \pi^0\pi^0$ candidates, its efficiency, and the measured $\mathcal{B}(D^0 \to \pi^0\pi^0)$ in Ref. [7], *BABAR* set an upper limit at 90% confidence level (CL) on the $D^0 \to \gamma\gamma$ branching fraction of $2.2 \times 10^{-6}$ which is the most stringent limit to date.

In this paper we report a search for $D^0 \to \gamma\gamma$ using $2.92 \pm 0.03$ fb$^{-1}$ of $e^+e^-$ annihilation data collected by the BESIII detector [9] at $\sqrt{s} = 3.773$ GeV in 2010 and 2011. There are about 20 million $D^0$ mesons produced [10] from $\psi(3770)$ decays in this sample. Taking advantage of the fact that $D$-meson production near the $\psi(3770)$ resonance is solely through $D\bar{D}$, we apply a tagged technique pioneered by the MARK III Collaboration [11]. After reconstructing a hadronically decaying $\bar{D}$ in an event (the tag), we then search for $D$-decay candidates of interest in the remainder of the event. (Unless otherwise noted, charge conjugate modes are implied throughout this paper.) This strategy suppresses background and provides an absolute normalization for branching fraction measurements independent of the integrated luminosity and $D\bar{D}$ production cross section. Therefore, searches for $D^0 \to \gamma\gamma$ with BESIII at open-charm threshold are uniquely clean and provide a valuable complement to studies at the $\Upsilon(4S)$.

In addition to our primary result, we also report an improved measurement of the branching fraction for the decay $D^0 \to \pi^0\pi^0$, which is the dominant background for $D^0 \to \gamma\gamma$. Precise measurement of the $D^0 \to \pi^0\pi^0$ branching fraction can improve understanding of U-spin and SU(3)-flavor symmetry breaking effects in $D^0$ decays [12], benefiting theoretical predictions of $CP$ violation in $D$ decays [13].

## II. THE BESIII DETECTOR AND MONTE CARLO SIMULATIONS

The data used in this analysis were collected with the BESIII detector operating at the BEPCII Collider. The BESIII detector, which is described in detail elsewhere [14], has a geometrical acceptance of 93% of $4\pi$ and consists of four main components. A small-celled, helium-based, multilayer drift chamber (MDC) with 43 layers provides momentum resolution for 1-GeV/$c$ charged particles in a 1-T magnetic field of 0.5%. Excellent charged particle identification is achieved by utilizing the energy loss in the MDC ($dE/dx$). A time-of-flight system (TOF) for additional charged particle identification is composed of plastic scintillators. The time resolution is 80 ps in the barrel and 110 ps in the endcaps, giving $2\sigma K/\pi$ separation for momenta up to about 1 GeV/$c$. An electromagnetic calorimeter (EMC) is constructed of 6240 CsI (Tl) crystals arranged in a cylindrical shape (barrel) plus two endcaps. For 1.0-GeV photons, the energy resolution is 2.5% in the barrel and 5% in the endcaps. Finally, a muon chamber system (MUC) is constructed of resistive plate chambers. These are interleaved with the flux-return iron of the superconducting magnet.

Monte Carlo (MC) simulations are used for efficiency and background determinations. Events are generated with

KKMC [15], which incorporates initial-state radiation and the spread of the BEPCII beam energy. The generated particles are subsequently passed to EVTGEN [16], which simulates particle decays based on known branching fractions [17]. To realistically mimic our data, we produce a generic MC sample including $e^+e^- \to \psi(3770) \to D\bar{D}$, continuum hadron production ($e^+e^- \to \gamma^* \to q\bar{q}$, with $q = u, d$ or $s$), radiative returns to the lower $c\bar{c}$ resonances ($e^+e^- \to \gamma_{\rm ISR}(\psi(3686)$ or $J/\psi)$), $e^+e^- \to \tau^+\tau^-$, and the doubly-radiative Bhabha process $e^+e^- \to e^+e^-\gamma\gamma$. The last component is generated with BABAYAGA [18]. We also generate a signal MC sample consisting of $e^+e^- \to \psi(3770) \to D^0\bar{D}^0$ events in which the $D^0$ or the $\bar{D}^0$ decays into a hadronic tag mode or $\gamma\gamma$, while the other $\bar{D}^0$ or $D^0$ decays without restriction. For all MC samples, generated events are processed with GEANT4 [19] to simulate the BESIII detector response.

## III. $D^0 \to \gamma\gamma$ ANALYSIS WITH DOUBLE-TAG METHOD

The $\psi(3770)$ resonance is below the threshold for $D\bar{D}\pi$ production, so the events from $e^+e^- \to \psi(3770) \to D\bar{D}$ have $D$ mesons with energies equal to the beam energy ($E_{\rm beam}$) and known momentum. Thus, to identify $\bar{D}^0$ candidate, we define the two variables $\Delta E$ and $M_{\rm BC}$, the beam-constrained mass:

$$\Delta E \equiv \sum_i E_i - E_{\rm beam},$$

$$M_{\rm BC} \equiv \sqrt{E^2_{\rm beam} - \left|\sum_i \vec{p}_i\right|^2},$$

where $E_i$ and $\vec{p}_i$ are the energies and momenta of the $\bar{D}^0$ decay products in the center-of-mass system of the $\psi(3770)$. For true $\bar{D}^0$ candidates, $\Delta E$ will be consistent with zero, and $M_{\rm BC}$ will be consistent with the $\overline{D}^0$ mass.

Single tag (ST) candidate events are selected by reconstructing a $\bar{D}^0$ in one of the following five hadronic final states: $\bar{D}^0 \to K^+\pi^-$, $K^+\pi^-\pi^0$, $K^+\pi^-\pi^+\pi^-$, $K^+\pi^-\pi^+\pi^-\pi^0$, and $K^+\pi^-\pi^0\pi^0$, constituting approximately 37% of all $\bar{D}^0$ decays [17]. The resolution of $M^{\rm tag}_{\rm BC}$ is about 2 MeV/$c^2$, dominated by the beam-energy spread. The $\Delta E^{\rm tag}$ resolutions are about 10 MeV and 15 MeV for final states consisting entirely of charged tracks and for those including a $\pi^0$, respectively. We search for $D^0 \to \gamma\gamma$ decays in these tagged events, thereby highly suppressing backgrounds from QED continuum processes, potential $\psi(3770) \to$ non-$D\bar{D}$ decays, as well as $D^+D^-$ decays. The fraction of double tag (DT) events, in which the $D^0$ is reconstructed as $D^0 \to \gamma\gamma$, determines the absolute branching fraction for the signal mode,

$$\mathcal{B}(D^0 \to \gamma\gamma) = \frac{N_{{\rm tag},\gamma\gamma}}{\sum_i N^i_{\rm tag} \cdot (\epsilon^i_{{\rm tag},\gamma\gamma}/\epsilon^i_{\rm tag})}.$$

In this expression $i$ runs over each of the five tag modes, $N_{\rm tag}$ and $\epsilon_{\rm tag}$ are the ST yield and reconstruction efficiency, and $N_{{\rm tag},\gamma\gamma}$ and $\epsilon_{{\rm tag},\gamma\gamma}$ are the yield and efficiency for the DT combination of a hadronic tag and a $D^0 \to \gamma\gamma$ decay.

### A. Single-tag selection and yields

For each tag mode, $\bar{D}^0$ candidates are reconstructed from all possible combinations of final-state particles, according to the following selection criteria. Momenta and impact parameters of charged tracks are measured by the MDC. Charged tracks are required to satisfy $|\cos\theta| < 0.93$, where $\theta$ is the polar angle with respect to the direction of the positron beam, and to have a closest approach to the interaction point within $\pm 10$ cm along the beam direction and within 1 cm in the plane perpendicular to the beam. Discrimination of charged pions from kaons is achieved by combining information about the normalized energy deposition ($dE/dx$) in the MDC with the flight-time measurement from the TOF. For a positive identification, the probability of the $\pi(K)$ hypothesis is required to be larger than that of the $K(\pi)$ hypothesis.

Electromagnetic showers are reconstructed from clusters of energy deposits in the EMC crystals and are required to be inconsistent with deposition by charged tracks [20]. The energy deposited in nearby TOF counters is included to improve the reconstruction efficiency and energy resolution. The shower energies are required to be greater than 25 MeV for the barrel region ($|\cos\theta| < 0.80$) and greater than 50 MeV for the endcaps ($0.84 < |\cos\theta| < 0.92$). Showers in the angular range between the barrel and endcaps are poorly reconstructed and excluded from the analysis. Cluster-timing requirements are used to suppress electronic noise and energy deposits unrelated to the event. For any tag mode with a $\pi^0$ in the final state, photon pairs are used to reconstruct $\pi^0$ candidates if the invariant mass satisfies $(115 < m_{\gamma\gamma} < 150)$ MeV/$c^2$. To improve resolution and reduce background, we constrain the invariant mass of each photon pair to the nominal $\pi^0$ mass.

For ST modes, we accept $\bar{D}^0$ candidates that satisfy the requirements $1.847 < M^{\rm tag}_{\rm BC} < 1.883$ GeV/$c^2$ and $|\Delta E^{\rm tag}| < 0.1$ GeV. In events with multiple tag candidates, the one candidate per mode with reconstructed energy closest to the beam energy is chosen [10]. We extract the ST yield for each tag mode and the combined yields of all five modes from fits to $M^{\rm tag}_{\rm BC}$ distributions in the samples described above. The signal shape is derived from the MC simulation which includes the effects of beam-energy smearing, initial-state radiation, the $\psi(3770)$ line shape, and detector resolution. We then convolute the line shape with a Gaussian to compensate for a difference in resolution between data and our MC simulation. Mean and width of the convoluted Gaussian, along with the overall normalization, are left free in our nominal fitting procedure. The background is described by an ARGUS function [21],

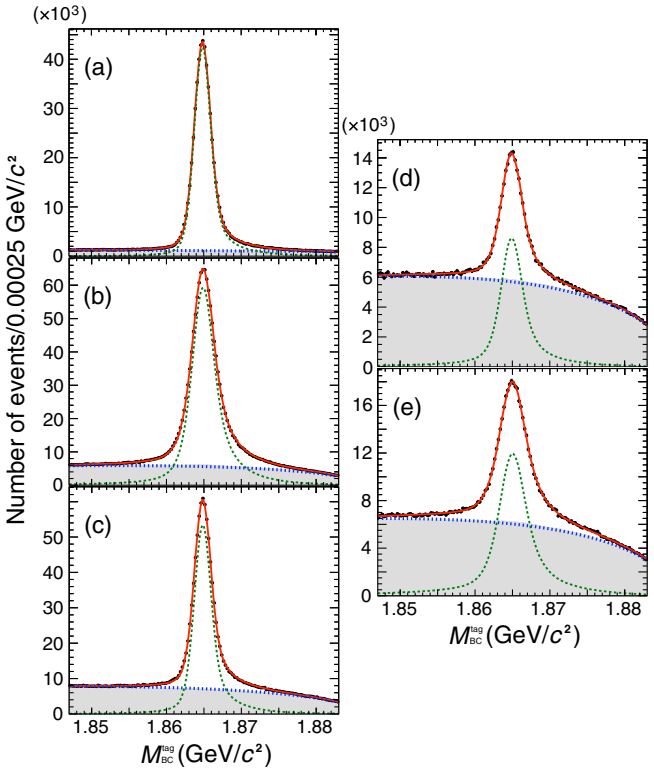


FIG. 1 (color online). Fits (solid line) to the $M_{\rm BC}^{\rm tag}$ distributions in data (points) for the five $\bar{D}^0$ tag modes: (a) $K^+\pi^-$, (b) $K^+\pi^-\pi^0$, (c) $K^+\pi^-\pi^+\pi^-$, (d) $K^+\pi^-\pi^+\pi^-\pi^0$, and (e) $K^+\pi^-\pi^0\pi^0$. The gray shaded histograms are arbitrarily scaled generic MC backgrounds.

which models combinatorial contributions. In the fit, we leave free all parameters of the background function, except its endpoint which is fixed at 1.8865 GeV/$c^2$. Figure 1 shows the fits to our tag-candidate samples. Tag yields, given in Table I, are obtained by subtracting the fitted background estimates from the overall fits in data within the narrow signal window $M_{\rm BC}^{\rm tag}$ ($1.858 < M_{\rm BC}^{\rm tag} < 1.874$ GeV/$c^2$). The total number of tags reconstructed in our data is approximately 2.8 million. Also shown in Table I are the tagging efficiencies obtained by fitting generic MC $M_{\rm BC}^{\rm tag}$ distributions with the same procedure used on data. These ST and DT efficiencies include the $\pi^0 \to \gamma\gamma$ branching fraction.

TABLE I. Single-tag efficiencies ($\epsilon_{\rm tag}^i$), tag yields ($N_{\rm tag}^i$) in data, double-tag efficiencies ($\epsilon_{{\rm tag},\gamma\gamma}^i$) and their statistical uncertainties. Efficiencies are determined based on MC simulations.

| modes | $\epsilon_{\rm tag}^i$ (%) | $N_{\rm tag}^i$ | $\epsilon_{{\rm tag},\gamma\gamma}^i$ (%) |
|---|---|---|---|
| $K^+\pi^-$ | $66.12 \pm 0.04$ | $551800 \pm 936$ | $44.8 \pm 0.4$ |
| $K^+\pi^-\pi^0$ | $35.06 \pm 0.02$ | $1097113 \pm 1386$ | $24.5 \pm 0.1$ |
| $K^+\pi^-\pi^+\pi^-$ | $39.70 \pm 0.03$ | $734825 \pm 1170$ | $24.7 \pm 0.2$ |
| $K^+\pi^-\pi^+\pi^-\pi^0$ | $15.32 \pm 0.04$ | $155899 \pm 872$ | $9.6 \pm 0.1$ |
| $K^+\pi^-\pi^0\pi^0$ | $15.23 \pm 0.04$ | $268832 \pm 976$ | $8.9 \pm 0.1$ |
| All Tags | | $2808469 \pm 2425$ | |

### B. Double-tag selection and yield

We select DT candidates by reconstructing $D^0 \to \gamma\gamma$ from the two most energetic photon candidates that are not used in reconstructing the tag mode. The selection criteria for these photons are the same as the ones used on the tag side, except that we require $0.86 < |\cos\theta| < 0.92$ for endcap showers to remove photons landing near the transition region. We require $|\Delta E^{\rm tag}| < 0.10$ GeV ($1.858 < M_{\rm BC}^{\rm tag} < 1.874$ GeV/$c^2$) and $|\Delta E^{\gamma\gamma}| < 0.25$ GeV ($M_{\rm BC}^{\gamma\gamma} > 1.85$ GeV/$c^2$) to the tag $\bar{D}^0$ candidate and the signal $D^0$ candidate, respectively. If there are multiple DT candidates, we choose the combination for which the average of $M_{\rm BC}^{\rm tag}$ and $M_{\rm BC}^{\gamma\gamma}$ ($\bar{M}_{\rm BC} \equiv (M_{\rm BC}^{\rm tag} + M_{\rm BC}^{\gamma\gamma})/2$) is closest to the known $D^0$ mass [10].

For any DT including $\bar{D}^0 \to K^+\pi^-$, the dominant background is from the doubly-radiative Bhabha QED process $e^+e^- \to e^+e^-\gamma\gamma$, which has a large production cross-section. To remove this background, we require the angle between the direction of the photon candidates and any charged tracks to be greater than 10 degrees. This requirement eliminates 93% of the QED background. For all tag modes, the dominant peaking background in the $\Delta E^{\gamma\gamma}$ signal region is from $D^0 \to \pi^0\pi^0$. To remove this background, we implement a $\pi^0$ veto. We reject events in which one of the $D^0 \to \gamma\gamma$ final-state photons can be combined with any other photon in the event to form a $\pi^0$. This requirement rejects 82% of the $D^0 \to \pi^0\pi^0$ background and keeps 88% of the signal events. Figure 2 shows the distributions of $\Delta E^{\gamma\gamma}$ (top) and $\Delta E^{\rm tag}$ (bottom) after the above selection criteria are applied, overlaid with the MC background estimate.

While we can suppress most of the background with the DT method, there remain residual contributions from continuum processes, primarily doubly-radiative Bhabha events for $K\pi$ tags and $e^+e^- \to q\bar{q}$ for other modes. In order to correctly estimate their sizes, we take a data-driven approach by performing an unbinned maximum likelihood fit to the two-dimensional distribution of $\Delta E^{\gamma\gamma}$ versus $\Delta E^{\rm tag}$. We use $\Delta E^{\gamma\gamma}$ distributions rather than $M_{\rm BC}^{\gamma\gamma}$ distributions as the background from non-$D\bar{D}$ decays is more easily addressed in the fit. Also, the background from $D^0 \to \pi^0\pi^0$ peaks in $M_{\rm BC}^{\gamma\gamma}$ at the same place as the signal does, whereas it is shifted in $\Delta E^{\gamma\gamma}$. The fitting ranges are $|\Delta E^{\gamma\gamma}| < 0.25$ GeV and $|\Delta E^{\rm tag}| < 0.1$ GeV. These wide ranges are chosen to have adequate statistics of the continuum backgrounds in our fit. The $\Delta E^{\gamma\gamma}$ resolution is 25 MeV, as determined with signal MC. For the signal and the $D^0 \to \pi^0\pi^0$ background, we extract probability density functions (PDFs) from MC, where the number of $D^0 \to \pi^0\pi^0$ background events is fixed to the result of the data-driven method described in Sec. IV. For the background from continuum processes, we include a flat component in two dimensions, allowing the normalization to float. The contribution from $D^+D^-$ decays is completely negligible. We model the background from other $D^0\bar{D}^0$ decays with a pair of functions. In the $\Delta E^{\rm tag}$ dimension we

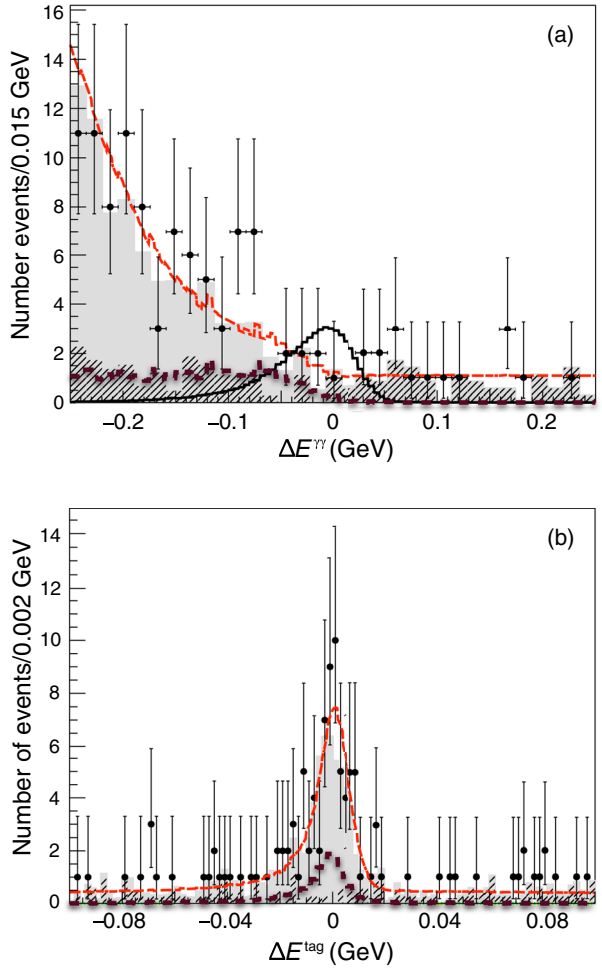


FIG. 2 (color online). Fit to the DT sample in data (points), projected onto $\Delta E^{\gamma\gamma}$ (a) and $\Delta E^{\rm tag}$ (b). The dashed lines show the overall fits, while the dotted histograms represent the estimated background contribution from $D^0 \to \pi^0\pi^0$. The solid line superimposed on the $\Delta E^{\gamma\gamma}$ projection indicates the expected signal for $\mathcal{B}(D^0 \to \gamma\gamma) = 10 \times 10^{-6}$. Also overlaid are the overall MC-estimated backgrounds (gray shaded histograms) and the background component from non-$D\bar{D}$ processes (diagonally hatched histograms).

use a Crystal Ball Line function (CBL) [22] plus a Gaussian, and in the $\Delta E^{\gamma\gamma}$ dimension, we use a second-order exponential polynomial:

$$Y(\Delta E^{\gamma\gamma}) = N \times e^{-(c_1\cdot\Delta E^{\gamma\gamma} + c_2\cdot(\Delta E^{\gamma\gamma})^2)}.$$

In our nominal fitting procedure, we fix the following parameters based on MC: the power-law tail parameters of the CBL, the coefficients ($c_1$ and $c_2$) of the above exponential polynomial, and the mean and the width of the Gaussian function. The normalization for the background from all other $D^0\bar{D}^0$ decays is left free in the fit, as are the mean and width of the CBL and the ratio of the areas of the CBL and Gaussian functions. Table I lists the DT signal-reconstruction efficiencies for each of the five tag modes.

As a test to validate the fitting procedure, we fit to 10,000 sets of pseudo-data (toy MC samples) generated by randomly distributing points based on our generic MC samples while taking into account the Poisson distribution with input $D^0 \to \gamma\gamma$ branching fractions of $(0, 5, 10) \times 10^{-6}$. The average branching fractions measured with these samples are $(0.3 \pm 1.2, 5.0 \pm 2.4, 10.0 \pm 3.1) \times 10^{-6}$, respectively, where the quoted uncertainties are the root-mean-squares of the distributions.

Figure 2 shows projections of the fit to the DT data sample onto $\Delta E^{\gamma\gamma}$ (top) and $\Delta E^{\rm tag}$ (bottom). We also overlay background distributions predicted by the MC simulations. The fit yields $N_{{\rm tag},\gamma\gamma} = (-1.0^{+3.7}_{-2.3})$, demonstrating that there is no signal for $D^0 \to \gamma\gamma$ in our data. This corresponds to $\mathcal{B}(D^0 \to \gamma\gamma) = (-0.6^{+2.0}_{-1.3}) \times 10^{-6}$ where the uncertainties are statistical only.

## IV. SIZE OF $D^0 \to \pi^0\pi^0$ BACKGROUND

To estimate the contribution of background from $D^0 \to \pi^0\pi^0$ events to our selection, we make a second DT measurement with the same sample used in searching for $D^0 \to \gamma\gamma$. Within these tagged events, we reconstruct $D^0 \to \pi^0\pi^0$ with the $\pi^0$ candidates that are not used in reconstructing the tag modes. The selection criteria for these $\pi^0$ candidates are the same as those used in reconstructing the tags. We select the pair of $\pi^0$ s that gives the smallest $|\Delta E^{\pi^0\pi^0}|$ and extract the DT yield by fitting to $M_{\rm BC}^{\pi^0\pi^0}$, while requiring $-0.070 < \Delta E^{\pi^0\pi^0} < +0.075$ GeV. In this fit, a double-Gaussian function is used to represent the $M_{\rm BC}^{\pi^0\pi^0}$ shape for the $D^0 \to \pi^0\pi^0$ decays, while the $D^0\bar{D}^0$ MC shape describes the background.

Figure 3 shows the fit to the $M_{\rm BC}^{\pi^0\pi^0}$ distribution in $1.840 < M_{\rm BC}^{\pi^0\pi^0} < 1.886$ GeV/$c^2$, which yields $N_{\pi^0\pi^0}^{\rm obs} = 1036 \pm 35$ events for $D^0 \to \pi^0\pi^0$. Thus the yield in our data sample of $D^0 \to \pi^0\pi^0$ with a $\bar{D}^0$ decaying into one of the five tag modes is $N_{\pi^0\pi^0}^{\rm produced} = N_{\pi^0\pi^0}^{\rm obs}/\epsilon_{\rm DT}^{\pi^0\pi^0}$, where $\epsilon_{\rm DT}^{\pi^0\pi^0} = 6.08\%$ is the DT efficiency for $D^0 \to \pi^0\pi^0$ as determined with MC. The expected $\pi^0\pi^0$ contribution to our $\gamma\gamma$ candidates can be then obtained as

$$N_{\pi^0\pi^0}^{\rm expected} = N_{\pi^0\pi^0}^{\rm produced} \times \epsilon_{\pi^0\pi^0}^{\gamma\gamma} = N_{\pi^0\pi^0}^{\rm obs} \frac{\epsilon_{\pi^0\pi^0}^{\gamma\gamma}}{\epsilon_{\rm DT}^{\pi^0\pi^0}}$$

where $\epsilon_{\pi^0\pi^0}^{\gamma\gamma} = 0.11\%$ is the efficiency for $D^0 \to \pi^0\pi^0$ to be counted as $D^0 \to \gamma\gamma$. The efficiencies $\epsilon_{\pi^0\pi^0}^{\gamma\gamma}$ and $\epsilon_{\rm DT}^{\pi^0\pi^0}$ include the reconstruction efficiencies for the tag sides as well as the branching fractions, although these cancel in the ratio.

We consider the following sources of systematic uncertainty in determining the $D^0 \to \pi^0\pi^0$ contamination: $\pi^0$ reconstruction (1.5%), photon reconstruction (2.0%), binning of $M_{\rm BC}^{\pi^0\pi^0}$ (0.1%), fit range (0.1%), background shape

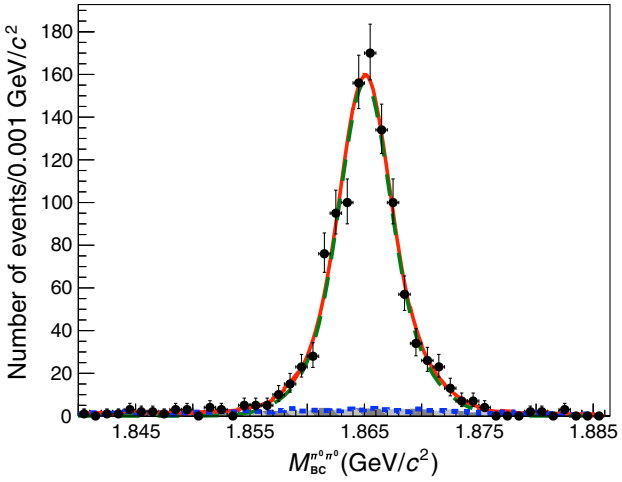


FIG. 3 (color online). Fit to the $M_{\rm BC}^{\pi^0\pi^0}$ distribution in data (points) for $D^0 \to \pi^0\pi^0$ DT candidates. The solid line is the total fitted result, while the dotted and dashed lines are the background and signal components of the fit, respectively. The diagonally shaded histogram is the background determined with MC.

(0.5%), signal shape (1.7%), and the $\Delta E^{\pi^0\pi^0}$ requirement (0.6%). Combining statistical and systematic uncertainties, we estimate the number of $D^0 \to \pi^0\pi^0$ events among the $D^0 \to \gamma\gamma$ candidates to be 18 events with a relative uncertainty of 4.6%, spread across the $\Delta E^{\gamma\gamma}$ fit range.

## V. SYSTEMATIC UNCERTAINTIES FOR $D^0 \to \gamma\gamma$ ANALYSIS

MC studies demonstrate that $D$-decay measurements based on DT-to-ST ratios benefit from cancellation of most of the systematic uncertainties of tag reconstruction. The overall systematic uncertainty in our measurement is therefore dominated by other effects. The systematic uncertainties that are independent of our signal-fitting procedure are that associated with detection of the two photons, which is estimated by studying the reconstruction efficiency of a daughter photon from $\pi^0$ decay in a DT $D^0 \to K_S^0\pi^0$ sample (2.0%); the signal-side $M_{\rm BC}^{\gamma\gamma}$ requirement, which is estimated from the $\Delta E^{\pi^0\pi^0}$ distribution of the DT $D^0 \to \pi^0\pi^0$ sample and by observing the stability of the $\mathcal{B}(D^0 \to \pi^0\pi^0)$ while varying the selected range of $M_{\rm BC}^{\pi^0\pi^0}$ (3.1%). The systematic uncertainties in ST yields (1.0%) are estimated first for individual tag modes, and then combined in quadrature with weights based on the observed tag yields ($N_{\rm tag}^i$). The sources for the uncertainties of ST yields we consider are the choice of fit range, assumed signal parametrization, and the $M_{\rm BC}^{\rm tag}$ signal window. Combined in quadrature, these total 3.8%.

We also consider six possible sources of systematic effects due to our fitting procedure. (i) Fits are redone with all possible combinations of fitting ranges: $-(0.12, 0.10, 0.08) < \Delta E^{\rm tag} < +(0.08, 0.10, 0.12)$ GeV and $-(0.30, 0.25, 0.20) < \Delta E^{\gamma\gamma} < +(0.20, 0.25, 0.30)$ GeV. (ii) The MC-based analytic form of the $D^0\bar{D}^0$ background shape (excluding the $D^0 \to \pi^0\pi^0$ contribution) is varied by changing the input branching fractions for $D^0 \to \pi^0\eta/\eta\eta/K_L^0\eta/K_L^0\pi^0$ by $\pm 1\sigma_{\rm PDG}$ [17]. (iii) The flat non-$D\bar{D}$ background shape is replaced with a shape that is linear in the $\Delta E^{\gamma\gamma}$ dimension. (iv) The fixed size of the background from $D^0 \to \pi^0\pi^0$ is varied by $\pm 4.6\%$. (v) The fixed shape of the background from $D^0 \to \pi^0\pi^0$ is studied by comparing $\Delta E$ distributions of DT events from $D^0 \to \pi^0\pi^0/K_S^0\pi^0/K\pi\pi^0$ between data and MC simulations in which we intentionally ignore the lower-energy photon from each $\pi^0$ decay to mimic our background. We conclude that we do not need to assign additional systematic uncertainty due to the assumed $D^0 \to \pi^0\pi^0$ background shape in the fit, except to give an extra Gaussian smearing of $\sigma = 5$ MeV in the $\Delta E^{\rm tag}$ dimension. (vi) The fixed signal shape is studied based on the DT $D^0 \to \pi^0\pi^0$ sample in which we study distributions of its $\Delta E^{\rm tag}$ and $\Delta E^{\pi^0\pi^0}$ for four cases by requiring that one of the two photons from each of the two $\pi^0$ to have at least 0.5, 0.6, 0.7, and 0.8 GeV to mimic our signal photon energies. From all four cases, we find that we need an extra Gaussian smearing of $\sigma = 16$ MeV and a shift by a factor of 1.0025 in the $\Delta E^{\gamma\gamma}$ dimension as well as an extra smearing of $\sigma = 5$ MeV in the $\Delta E^{\rm tag}$ dimension.

Table II summarizes systematic uncertainties that are independent of our fitting procedure, as well as systematic variations that we consider to estimate uncertainties due to the fitting procedure. In the next section, we describe how we combine these systematic uncertainties into our measurement.

TABLE II. Systematic uncertainties and variations for $D^0 \to \gamma\gamma$ analysis.

| Uncertainties independent of fitting procedure | |
|---|---|
| Source | Relative uncertainty (%) |
| Photon reconstruction | 2.0 |
| $M_{\rm BC}^{\gamma\gamma}$ requirement | 3.1 |
| ST $D^0$ yields | 1.0 |
| Total | 3.8 |

| Systematic variations due to fitting procedure | |
|---|---|
| Source | Variations |
| Fit range (GeV) | $\pm 0.02$ in $E^{\rm tag}$ and $\pm 0.05$ in $E^{\gamma\gamma}$ |
| $D^0 \to \pi^0\pi^0$ norm. | $\pm 4.6\%$ |
| $D^0 \to \pi^0\pi^0$ shape | Smear in $\Delta E^{\rm tag}$ |
| $D^0\bar{D}^0$ bkg shape | $\Delta\mathcal{B}_{\rm input}[D^0 \to (\eta\pi^0/\eta\eta/K_L^0\pi^0/K_L^0\eta)]$ |
| Non-$D^0\bar{D}^0$ bkg shape | Flat vs Linear |
| Signal shape | Smear in $\Delta E^{\rm tag}$ and $\Delta E^{\gamma\gamma}$, shift in $E^{\gamma\gamma}$ |

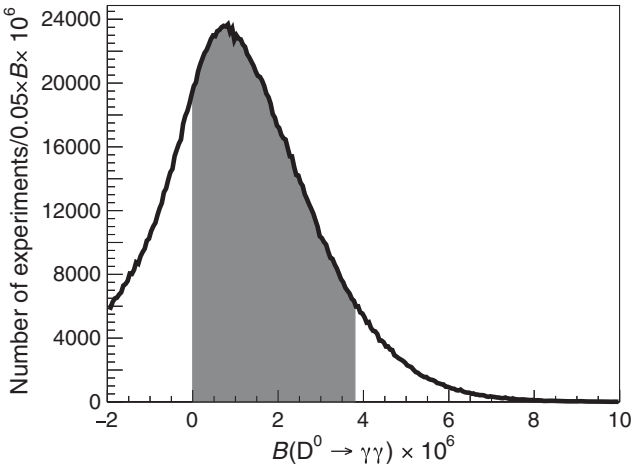


FIG. 4. Accumulated branching fraction distribution based on toy MC samples generated from the data-driven PDF. (See the text for details.) The shaded region represents 90% of the physical region.

## VI. THE RESULT FOR $D^0 \to \gamma\gamma$

Since we do not observe a signal, we set an upper limit on the branching fraction for $D^0 \to \gamma\gamma$. We first obtain a smooth background-only PDF shape from the sample via the kernel estimation method [23]. This is done by utilizing the RooFit class [24] RooNDKeysPdf [25]. We then generate 2.2 million toy MC samples by randomly distributing points according to the PDF shape, while taking into account the Poisson distribution. We fit to each of these toy samples while randomly making systematic variations in the fitting procedure, as described in the previous section. We also simultaneously smear each of the fitted branching fractions with a Gaussian whose width (3.8%) corresponds to the total systematic uncertainty that is not associated with the fitting procedure.

Figure 4 shows an accumulation of the resulting branching fractions for $D^0 \to \gamma\gamma$. The shaded region represents 90% of its physical region, which we use to set our 90% CL upper limit of $\mathcal{B}(D^0 \to \gamma\gamma) < 3.8 \times 10^{-6}$. If the systematic uncertainty were ignored in setting this limit it would be reduced by $0.1 \times 10^{-6}$. The expected measurement of branching fraction from these toy experiments is $(+0.7^{+2.0}_{-2.5}) \times 10^{-6}$, where the quoted uncertainties correspond to 68% of the areas under the curves in Fig. 4. The mean value of the accumulated branching fractions is consistent with the value of the branching fraction from the nominal fit to data at $0.6\sigma$ level.

## VII. IMPROVED MEASUREMENT OF $D^0 \to \pi^0\pi^0$ BRANCHING FRACTION

As a byproduct of this analysis we also measure the branching fraction of $D^0 \to \pi^0\pi^0$ using the same data sample. Since the produced $D^0\bar{D}^0$ pairs in our sample necessarily have opposite $CP$ eigenvalues [20], the effective branching fraction for the $CP$-even final state $\pi^0\pi^0$ is altered when it is measured in events tagged with a $CP$-mixed state such as $\bar{D}^0 \to K^+\pi^-$ [26]. To avoid this complication and to improve the statistics, instead of a DT technique, we reconstruct only one $D^0$ or $\bar{D}^0$ decay in the $\psi(3770) \to D^0\bar{D}^0$ process. The observed yield is normalized to the total number of the $D^0\bar{D}^0$ pairs, which can be obtained as $N_{D^0\bar{D}^0} = \mathcal{L} \times \sigma(e^+e^- \to \psi(3770) \to D^0\bar{D}^0)$, using the integrated luminosity $\mathcal{L}$ of our sample [9] and the previously measured cross section $\sigma(e^+e^- \to D^0\bar{D}^0) = (3.607 \pm 0.017(\text{stat}) \pm 0.056(\text{syst}))$ nb [10]. The branching fraction for $D^0 \to \pi^0\pi^0$ can be calculated as

$$\mathcal{B}(D^0 \to \pi^0\pi^0) = \frac{N_{\pi^0\pi^0}}{\epsilon_{\pi^0\pi^0} \cdot 2N_{D^0\bar{D}^0}},$$

where $N_{\pi^0\pi^0}$ is the observed number of $D^0 \to \pi^0\pi^0$ decays and $\epsilon_{\pi^0\pi^0}$ is the selection efficiency determined with MC.

The reconstruction of $\pi^0$ candidates is the same as those in the ST modes described in Sec. III A. We choose a pair of reconstructed $\pi^0$ s that give the smallest $|\Delta E^{\pi^0\pi^0}|$, and require $-0.06 < \Delta E^{\pi^0\pi^0} < +0.03$ GeV. The resolution of $\Delta E^{\pi^0\pi^0}$ is about 20 MeV. Then we extract the signal yield from a fit to $M_{\rm BC}^{\pi^0\pi^0}$. The efficiency is determined to be $\epsilon_{\pi^0\pi^0} = 36\%$ from MC simulations.

Figure 5 shows a fit to the $M_{\rm BC}^{\pi^0\pi^0}$ distribution in $1.8400 < M_{\rm BC}^{\pi^0\pi^0} < 1.8865$ GeV/$c^2$. We use a double-Gaussian function to describe the signal shape, which is shown as a dotted line, and the background shape is described by an ARGUS background function [21]. From this fit, which yields $\chi^2/\text{d.o.f.} = 91.8/85$, we obtain $N_{\pi^0\pi^0} = 6277 \pm 156$ events. In Fig. 5, we also overlay the

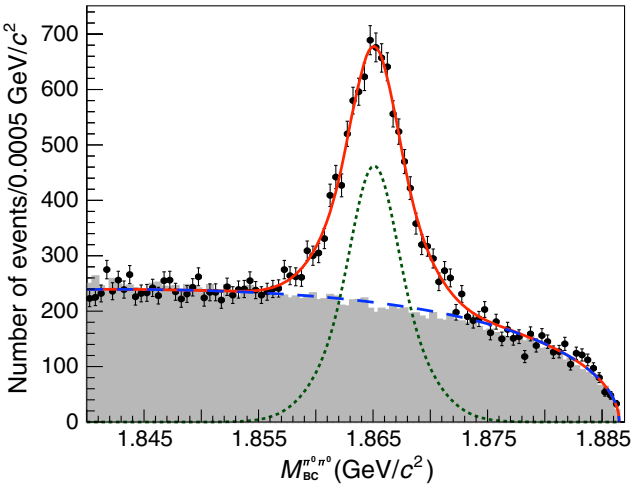


FIG. 5 (color online). Fit to the $M_{\rm BC}^{\pi^0\pi^0}$ distribution in data for $D^0 \to \pi^0\pi^0$ candidates (points). The shaded histogram is the background predicted by MC. The solid and dashed curves are the total fit and the background component, respectively, and the dotted curve shows the signal.

TABLE III. Systematic uncertainties for $D^0 \to \pi^0\pi^0$ analysis.

| Source | Relative uncertainty (%) |
|---|---|
| $\pi^0$ reconstruction | 1.5 |
| Histogram binning | 0.1 |
| Fit range | 2.4 |
| $\Delta E^{\pi^0\pi^0}$ requirement | 0.6 |
| Background shape | 0.2 |
| Signal shape | 0.9 |
| $N_{D^0\bar{D}^0}$ | 1.9 |
| Total | 3.6 |

backgrounds that are estimated by the MC simulations (gray shaded histogram).

From the fitted signal yields ($N_{\pi^0\pi^0}$) and reconstruction efficiency ($\epsilon_{\pi^0\pi^0}$), we obtain

$$\mathcal{B}(D^0 \to \pi^0\pi^0) = (8.24 \pm 0.21(\text{stat}) \pm 0.30(\text{syst})) \times 10^{-4}.$$

The quoted total systematic uncertainty (3.6%) is the quadrature sum of the following seven sources of uncertainty. (i) The uncertainty due to $\pi^0$ reconstruction is estimated with a DT $D^0 \to K^-\pi^+\pi^0$ sample. (ii) Histogram binning scheme is varied. (iii) Narrower ($1.8450 < M_{\text{BC}}^{\pi^0\pi^0} < 1.8820$ GeV/$c^2$) and broader ($1.8350 < M_{\text{BC}}^{\pi^0\pi^0} < 1.8865$ GeV/$c^2$) fit ranges are tried. (iv) Narrower ($-0.055 < \Delta E^{\pi^0\pi^0} < 0.025$ GeV) and broader ($-0.065 < \Delta E^{\pi^0\pi^0} < 0.035$ GeV) requirements are applied. (v) Instead of using the ARGUS function [21], a MC-based background shape is used. (vi) To assess a possible bias due to the signal line shape, we fix the all shape parameters of the double Gaussians based on the shape extracted from the DT $D^0 \to K^-\pi^+\pi^0$ sample. (vii) The uncertainty of the determination of $N_{D^0\bar{D}^0}$ is determined based on Refs. [9,10]. The resultant relative uncertainties are shown in Table III.

## VIII. CONCLUSIONS

Using 2.92 fb$^{-1}$ of $e^+e^-$ annihilation data collected at $\sqrt{s} = 3.773$ GeV with the BESIII detector, we have searched for the FCNC decay $D^0 \to \gamma\gamma$ and observe no significant signal. We set an upper limit $\mathcal{B}(D^0 \to \gamma\gamma) < 3.8 \times 10^{-6}$ at the 90% CL, which is consistent with the upper limit previously set by the *BABAR* Collaboration [7] and with the SM prediction. Ours is the first experimental study of this decay using data at open-charm threshold. Employing the DT technique, we are able to suppress the backgrounds from non-$D\bar{D}$ decays effectively. Our analysis also shows that the peaking background from $D^0 \to \pi^0\pi^0$ can be reliably estimated with a data-driven method.

We have also measured the branching fraction for $D^0 \to \pi^0\pi^0$ to be $(8.24 \pm 0.21(\text{stat}) \pm 0.30(\text{syst})) \times 10^{-4}$ which is consistent with the previous measurements [27] and the most precise to date.

## ACKNOWLEDGMENTS

The BESIII collaboration thanks the staff of BEPCII and the IHEP computing center for their strong support. This work is supported in part by National Key Basic Research Program of China under Contract No. 2015CB856700; National Natural Science Foundation of China (NSFC) under Contracts Nos. 11125525, 11235011, 11322544, 11335008, 11425524; the Chinese Academy of Sciences (CAS) Large-Scale Scientific Facility Program; Joint Large-Scale Scientific Facility Funds of the NSFC and CAS under Contracts Nos. 11179007, 11179014, U1232201, U1332201; CAS under Contracts Nos. KJCX2-YW-N29, KJCX2-YW-N45; 100 Talents Program of CAS; INPAC and Shanghai Key Laboratory for Particle Physics and Cosmology; German Research Foundation DFG under Contract No. Collaborative Research Center CRC-1044; Istituto Nazionale di Fisica Nucleare, Italy; Ministry of Development of Turkey under Contract No. DPT2006K-120470; Russian Foundation for Basic Research under Contract No. 14-07-91152; U.S. Department of Energy under Contracts Nos. DE-FG02-04ER41291, DE-FG02-05ER41374, DE-FG02-94ER40823, DESC0010118; U.S. National Science Foundation; University of Groningen (RuG) and the Helmholtzzentrum fuer Schwerionenforschung GmbH (GSI), Darmstadt; WCU Program of National Research Foundation of Korea under Contract No. R32-2008-000-10155-0.

[1] S. L. Glashow, J. Iliopoulos, and L. Maiani, Phys. Rev. D **2**, 1285 (1970).
[2] C. Greub, T. Hurth, M. Misiak, and D. Wyler, Phys. Lett. B **382**, 415 (1996).
[3] S. Fajfer, P. Singer, and J. Zupan, Phys. Rev. D **64**, 074008 (2001).
[4] G. Burdman, E. Golowich, J. A. Hewett, and S. Pakvasa, Phys. Rev. D **66**, 014009 (2002).
[5] S. Prelovsek and D. Wyler, Phys. Lett. B **500**, 304 (2001).
[6] A. Paul, I. I. Bigi, and S. Recksiegel, Phys. Rev. D **82**, 094006 (2010).

[7] J. P. Lees *et al.* (*BABAR* Collaboration), Phys. Rev. D **85**, 091107(R) (2012).
[8] T. E. Coan *et al.* (CLEO Collaboration), Phys. Rev. Lett. **90**, 101801 (2003).
[9] M. Ablikim *et al.* (BESIII Collaboration), Chin. Phys. C **37**, 123001 (2013).
[10] Q. He *et al.* (CLEO Collaboration), Phys. Rev. Lett. **95**, 121801 (2005); **96**, 199903(E) (2006); S. Dobbs *et al.* (CLEO Collaboration), Phys. Rev. D **76**, 112001 (2007); G. Bonvicini *et al.* (CLEO Collaboration), Phys. Rev. D **89**, 072002 (2014); **91**, 019903(E) (2015).
[11] R. M. Baltrusaitis *et al.* (MARK III Collaboration), Phys. Rev. Lett. **56**, 2140 (1986).
[12] W. Kwong and S. P. Rosen, Phys. Lett. B **298**, 413 (1993); Y. Grossman and D. J. Robinson, J. High Energy Phys. 04 (2013) 067.
[13] Y. Grossman, A. L. Kagan, and J. Zupan, Phys. Rev. D **85**, 114036 (2012).
[14] M. Ablikim *et al.* (BESIII Collaboration), Nucl. Instrum. Methods Phys. Res., Sect. A **614**, 345 (2010).
[15] S. Jadach, B. F. L. Ward, and Z. Was, Phys. Rev. D **63**, 113009 (2001).
[16] D. J. Lange, Nucl. Instrum. Methods Phys. Res., Sect. A **462**, 152 (2001); R. G. Ping, Chin. Phys. A **32**, 243 (2008).
[17] K. Nakamura *et al.* (Particle Data Group), J. Phys. G **37**, 075021 (2010) and 2011 partial update for the 2012 edition.
[18] C. M. C. Calame, C. Lunardini, G. Montagna, O. Nicrosini, and F. Piccinini, Nucl. Phys. **B584**, 459(2000); Phys. Lett. B **520**, 16 (2001); Nucl. Phys. B, Proc. Suppl. **131**, 48 (2004); G. Balossini, C. M. C. Calame, G. Montagna, O. Nicrosini, and F. Piccinini, Nucl. Phys. **B758**, 227 (2006); Phys. Lett. B **663**, 209 (2008).
[19] S. Agostinelli *et al.*, Nucl. Instrum. Methods Phys. Res., Sect. A **506**, 250 (2003); J. Allison *et al.*, IEEE Trans. Nucl. Sci. **53**, 270 (2006); Z. Y. Deng *et al.*, High Energy Phys. Nucl. Phys. **30**, 371 (2006).
[20] M. Ablikim *et al.* (BESIII Collaboration), Phys. Lett. B **744**, 339 (2015).
[21] H. Albrecht *et al.* (ARGUS Collaboration), Phys. Lett. B **241**, 278 (1990).
[22] J. E. Gaiser, Ph.D. thesis, Stanford Linear Accelerator Center, Stanford University, Stanford, California [Report No. SLAC-R-255, 1982 (unpublished)]; T. Skwarnicki, Ph.D. thesis, Institute of Nuclear Physics, Krakow, Poland [Report No. DESY-F31-86-02, 1986 (unpublished)].
[23] Kyle S. Cranmer, Comput. Phys. Commun. **136**, 198 (2001).
[24] W. Verkerke and D. Kirkby, eConf No. C0303241 (2003) MOLT007 [arXiv:physics/0306116].
[25] https://root.cern.ch/root/html/RooNDKeysPdf.html.
[26] D. M. Asner *et al.* (CLEO Collaboration), Phys. Rev. D **86**, 112001 (2012).
[27] K. A. Olive *et al.* (Particle Data Group), Chin. Phys. C **38**, 090001 (2014).